

**Energy accumulation in easterly circumpolar jets
generated by two-dimensional barotropic decaying
turbulence on a rapidly rotating sphere**

Shin-ichi Takehiro*, Michio Yamada

Research Institute for Mathematical Sciences, Kyoto University,

Sakyo-ku, Kyoto 606-8502, Japan

and

Yoshi-Yuki Hayashi

Graduate School of Science, Hokkaido University,

Sapporo 060-0810, Japan

December 9, 2006

*Email:takepiro@gfd-dennou.org

Abstract

A series of numerical experiments on two-dimensional decaying turbulence is performed for a barotropic fluid on a rotating sphere. Numerical calculations have confirmed two important asymptotic features; emergence of the banded structure of zonal flows and their extreme latitudinal inhomogeneities in which kinetic energy is accumulated into the easterly circumpolar jets. The banded structure of zonal flows is established relatively early on in the initial stage. Later, after extended periods of time integration, only the circumpolar jets are intensified gradually, while there is no further evolution in the banded structure in the low and mid-latitudes. Wave activity flux analysis illustrates that the initial vortices in the low and mid-latitudes propagate poleward as Rossby waves and converge to produce easterly circumpolar flows. In association with this convergence, accumulation of the mean zonal component of kinetic energy proceeds. The tendency for the accumulation becomes strong as the rotation rate is increased, and nearly all of the kinetic energy is concentrated to the circumpolar flows in cases of rapid rotation.

A theoretical model is constructed under the assumption that a circumpolar jet emerges around the latitude where the local Rhines scale is equal to the distance from the pole, and that initial vortices at the lower latitudes contribute to the generation of the jets. The model describes the mean zonal component of kinetic energy and the averaged speed and width of the circumpolar jets as functions of the rotation rate, which agree satisfactorily with the numerical results.

1. Introduction

Banded structures and associated zonal flows of planetary atmospheres, typically observed in Jovian planets, are one of the prominent planetary-scale fluid dynamical phenomena, and have attracted the interests of many researchers. Some of the studies have sought their generation and maintenance mechanism in deep convective motion (ex. Busse 1983, Heimpel *et al.* 2005), while others have extensively discussed the dynamical properties of two-dimensional fluid motions in a surface thin layer under the influence of rotation and stratification in relation to the emergence and maintenance of banded structures (ex. Rhines, 1975; Williams, 1978; Cho and Polvani, 1996; Li and Montgomery, 1996; 1997; Nozawa and Yoden, 1997a,b; Huang and Robinson 1998; Taniguchi *et al.*, 2002).

Among such attempts, the two-dimensional decaying turbulence on a rotating sphere is one of the basic problems of the most idealistic setups. Yoden and Yamada (1993) first performed numerical experiments of decaying turbulence on a rotating sphere with full spherical geometry. They investigated the statistical tendency for the development of a flow field from a random set of initial states, and found that a banded structure of zonal flows emerges and that there was a tendency for circumpolar flows to be easterly jets. However, especially in cases when the rotation rate is large, their initial fields are in a state of 'wave turbulence', that is, the initial kinetic energy spectrum is concentrated around the total wavenumber that is lower than the characteristic "Rhines wavenumber," at which the magnitudes of the linear and nonlinear terms are on the same order. Later, by using a higher resolution model, Ishioka *et al.* (1999) and Yoden *et al.* (1999) performed time integration from initial states with kinetic energy spectra

concentrated around the higher total wavenumbers and confirmed the emergence of the banded structure and the circumpolar easterly jets. They also found a decreasing trend in the width of the circumpolar jet and the bands with increase in rotation rate (for a more detailed review of these studies, see also Hayashi *et al.*, 2007).

Since these numerical observations were only qualitative, Takehiro *et al.* (2007) conducted a quantitative investigation on the strength and width of the easterly circumpolar jets and, by performing a series of experiments with longer time integration and larger rotation rates than the previous studies, discovered asymptotic behaviors in rapidly rotating cases. The integration periods of the preceding studies seemed to have been insufficient to fully develop the calculated flow fields, which were still developing at the end of the computations. Numerical calculations in Takehiro *et al.* (2007) revealed that the banded structure of zonal flows is extremely inhomogeneous and that most of the kinetic energy is accumulated inside the easterly circumpolar jets. It was argued that the averaged speed and width of the circumpolar jet are proportional to one-fourth power and minus one-fourth power of the rotation rate, respectively, in the asymptotic limits of large rotation rates.

In this paper, we extend the study of Takehiro *et al.* (2007) and discuss not only the asymptotic features of the circumpolar jets but also the development of the structures by consulting the wave quantities. In Section 2, the model and setup of the experiment are presented again for the readers' convenience, and the numerical results are examined more specifically in Section 3. In order to clarify the origin of easterly circumpolar jets, Section 4 presents an analysis of wave activity performed from the viewpoint of Rossby wave propagation by using the ensemble

average with 50 members. In Section 5, a theoretical model of kinetic energy accumulation is constructed and is compared with the numerical results. Section 6 summarizes our conclusions.

2. Model and setup for numerical experiments

The model and experiment setups are basically the same as that of Takehiro *et al.* (2007). Two-dimensional barotropic flow on a rotating sphere is governed by the vorticity equation for the vertical component of vorticity in the rotating frame of reference:

$$\frac{\partial \zeta}{\partial t} + J(\psi, \zeta) + 2\Omega \frac{\partial \psi}{\partial \lambda} = (-1)^{p+1} \nu_{2p} (\nabla^2 + 2)^p \zeta, \quad (1)$$

where $\psi(\lambda, \mu, t)$ is the stream function the sign of which follows the geophysical convention, $\zeta(\lambda, \mu, t)$ is the vertical component of vorticity ($= \nabla^2 \psi$), t is time, λ is longitude, and Ω is the rotation rate of the sphere. The nonlinear term $J(f, g) \equiv (\partial_\lambda f)(\partial_\mu g) - (\partial_\mu f)(\partial_\lambda g)$ is the horizontal Jacobian and $\mu = \sin \varphi$ with φ representing latitude. ν_{2p} is a coefficient of the hyperviscosity which we employ for the viscous dissipation occurring in a higher wavenumber range than in the case of the normal viscosity. Note that “2” in the parentheses of the hyperviscosity term ensures the conservation of angular momentum. In Eq.1, length, velocity, and time are non-dimensionalized with the radius of the sphere a , the characteristic velocity amplitude of the initial state U_0 (or square root of the mean kinetic energy $\sqrt{2\mathcal{E}}$), and the advection time scale a/U_0 , respectively. For numerical calculation, a spectral model of Eq.1 is constituted by expanding each physical variable into a series of spherical harmonic functions, and by truncat-

ing higher wavenumber components whose total wavenumbers are larger than N (Ishioka *et al.* 2000).

$$\psi(\lambda, \varphi, t) = \sum_{n=2}^N \sum_{m=-n}^n \tilde{\psi}_n^m(t) Y_n^m(\lambda, \varphi) \quad (2)$$

The nonlinear Jacobian term is computed with the spectral transform method, in which the nonlinear term is evaluated on physical space and transformed to spectral space each time. The core of the numerical model used in this study is available as “SPMODEL” of GFD Dennou Club, whose technical coding features are described in Takehiro *et al.* (2006).

For the numerical time integration, the linear terms are calculated analytically by transforming the variable with exponential factors, and the remaining nonlinear Jacobian term is dealt with by the fourth order Runge-Kutta method. The number of grid points on the physical space is 512 and 256 points in longitude and latitude, respectively, while the truncated total wavenumber N is set to 170 in order to avoid aliasing error in the nonlinear term. The parameters of the artificial hyperviscosity are selected as $p = 8$ and $\nu_{2p} = 10^{-34}$.

The initial velocity fields that we adopted in the simulation have the same spectral form of

$$E(n, t = 0) = \frac{An^{\gamma/2}}{(n + n_0)^\gamma}. \quad (3)$$

as those in Yoden *et al.* (1999), in which the kinetic energy spectrum is defined as $E(n, t) = (1/2)n(n + 1) \sum_{m=-n}^n |\tilde{\psi}_n^m(t)|^2$. Note that n_0 is the peak wavenumber of the kinetic energy spectrum, which is set to 50 here, and γ gives the width of the spectrum and takes the value of 100. We generated 25 initial velocity fields by using random numbers for amplitude and

phase of each coefficient of the spherical harmonics expansion, while retaining the above kinetic energy spectral form. The coefficient A is tuned to satisfy the condition that the mean kinetic energy be unity, *i.e.*, $\mathcal{E} = \sum_{n=2}^N E(n, t = 0) = 1$.

Studies preceding Takehiro *et al.* (2007) considered only the cases of $\Omega \leq 400$ (Ishioka *et al.*, 1999; Yoden *et al.*, 1999; Hayashi *et al.*, 2000; Yoden *et al.*, 2002). In the present study where the parameter space was expanded toward the rapid rotation side following Takehiro *et al.* (2007), we adopted $\Omega = 0, 50, 100, 200, 400, 1000, 4000$ and 10000 . For each rotation rate, we first performed time integration from 25 initial states. Then we analyzed the ensemble of the final flow fields, which was constructed from the 25 final fields from these runs and another 25 fields generated by reflecting the former 25 final fields with respect to the equator, resulting in 50 members in total. This procedure was performed to preserve the statistical reflection symmetry of the ensemble, taking into account the fact that the equation of motion is invariant to reflection with respect to the equator.

Time integrations were performed until the zonal flows are fully developed and their values of kinetic energy are saturated. The values of time increment and integration period are shown in Table 1. Note that the time developments were computed until $t = 5$ in the previous studies (Ishioka *et al.*, 1999; Yoden, *et al.*, 1999; Hayashi *et al.*, 2000; Yoden *et al.*, 2002). As is demonstrated in Takehiro *et al.* (2007) and will be shown later in this paper, the flow fields in previous studies were still developing at the end of the computation; thus, the final state of the mean zonal flows, especially those of the circumpolar jets could not be obtained from those earlier results.

[Table 1 about here.]

3. The results of individual numerical calculations

[Figure 1 about here.]

First, we will examine the results of individual developments of the fields. Many of the characteristics presented here have already been described by Takehiro *et al.* (2007), and hence, we will only present a brief summary for the convenience of readers. In addition to these, we emphasize here the inhomogeneous feature of the decaying turbulence on a rotating sphere, as is shown in the comparison of the zonal-mean zonal flow profiles between $t = 5$ and final state (Fig.2 right panels).

Fig.1 shows an example of the initial states. The kinetic energy spectrum is concentrated in the wavenumber zone located at the total wavenumber of 50 with width of about 20 wavenumbers. Small vortices corresponding to this spectrum are observed uniformly over the sphere. The amplitude of the mean zonal flow of the initial state is less than unity and the number of the bands, i.e., the number of maxima of easterlies and westerlies is also about 50, corresponding to the kinetic energy spectrum.

[Figure 2 about here.]

The left panels in Fig.2 show the vorticity fields of the final states when integration is started from the initial state given in Fig.1 using various values of Ω (the final time of each run is

listed in Table 1). When $\Omega = 0$ (not shown here, see Takehiro *et al.* 2007), the initial small vortices merge with each other into a few larger vortices surviving to the final state. When the system is rotating, a longitudinally elongated structure becomes predominant. As the rotation rate is increased, the longitudinal elongation becomes stronger and the width of the zonal band becomes narrower. However, in the case of $\Omega = 10000$, trains of small vortices whose aspect ratio is of the order of unity are found in the banded structure. Strong polar vortices also emerge when $\Omega \geq 400$, although they are barely seen in the figures.

The right panels in Fig.2 show the profiles of zonally averaged relative angular momentum at $t = 5$ and at the final stage. As already mentioned in the previous studies (Yoden *et al.* 1999, Ishioka *et al.* 1999 Hayashi *et al.* 2000), a banded structure of zonal flows in the low and mid-latitudes and circumpolar easterly jets in high latitudes emerge simultaneously at relatively early stages. A noteworthy point is that their later evolutions follow completely different paths.

The banded structure in the low and mid-latitudes are seldom developed further; the position and amplitude of each band does not change greatly, although a latitudinally uniform westerly acceleration with small amplitude does occur. On the other hand, the circumpolar easterly jets continue to grow into the late stage of the long integration periods, and become predominant over the banded structure in the low and mid-latitudes in the final state. The small but latitudinally uniform westerly bias observed in the low and mid-latitudes compensates the accumulation of easterly momentum in the polar caps.

It should be emphasized that, in the decaying turbulence on a rotating sphere, the banded structure of the zonal flows as a whole is extremely inhomogeneous in the latitudinal direction;

there are weak and slightly westerly biased banded zonal flows in the low and mid-latitude and intense easterly circumpolar jets. This tendency is enhanced as the rotation rate is increased. As seen in Fig.2 (b)-(d), the profiles of angular momentum of the circumpolar jets become sharp without accompanying changes in their amplitudes as the rotation rate is increased, while banded structures in the low and mid-latitudes become narrower and weaker.

The appearance of this extremely inhomogeneous feature in the evolution of zonal-mean zonal flow profile was not clearly described in the previous studies. The inhomogeneous feature and slow development of the circumpolar jets have been recognized in earlier studies such as Yoden and Yamada (1993), Yoden *et al.* (1999) and Hayashi *et al.* (2000). However, what was presented in their studies does not actually correspond to the present inhomogeneous feature of the banded structure, but to the robust appearance of the circumpolar easterly jets and the ensemble-averaging reduction of the amplitudes of randomly distributed zonal mean flows in the low and mid-latitudes (see also Fig.3). Moreover, since the final states of time integration of these studies were $t = 5$, at most, and the rotation rates utilized there were not so large, the zonal flows were still evolving and the accumulation of easterly momentum around the poles had not been completed. At $t = 5$ for $\Omega = 400$, indicated by the broken line in Fig.2b that corresponds to the final states of the largest rotation rate of Ishioka *et al.* (1999), Yoden *et al.* (1999), and Hayashi *et al.* (2000), the amplitudes of banded zonal flows in the low and mid-latitudes are comparable to those of the circumpolar jets. However, as the integration proceeds further, the circumpolar jets continue to grow, while the other zonal flows in the low and mid-latitudes are only slightly accelerated in the westerly direction. In the final state, after sufficiently long time

integration, at $t = 20$ for $\Omega = 400$ indicated by the solid line of Fig.2b, the easterly circumpolar jets dominate the zonal flows in the low and mid-latitudes. The time period required to achieve the final state decreases with increasing Ω . Fig.2d indicates that $t = 5$ can be regarded as the final state for the case of $\Omega = 10000$. It must be noted that, for the case of $\Omega = 10000$, the initial spectral energy peak is located at $n = 50$ and as is indicated by the characteristic wavenumber n_β (Nozawa and Yoden, 1997a) listed in Table 1, most of the domains except for the polar caps are regarded to be wavy like the case of $\Omega = 400$ of Yoden and Yamada (1993). However, we believe that, as in the case of $\Omega = 400$, if we start from an initial field having a higher wavenumber energy peak, we will still have the similar inhomogeneous feature of the banded zonal flows.

4. Results of the ensemble mean fields

As for the development of the circumpolar easterly jets, it has been suggested that the easterly momentum transport from the low and mid-latitudes associated with Rossby waves contributes to its maintenance (Hayashi *et al.* 2000, Hayashi *et al.* 2007). The problem, however, is that in order to illustrate the contribution of wave activity to the development of circumpolar zonal mean flow, a single time series of a run from a single initial state produces quite noisy wave-quantity profiles. Ensemble average may reduce such fluctuations caused by phase configurations of particular disturbances that appear in individual runs.

[Figure 3 about here.]

Before getting into the profiles of wave properties, let us briefly summarize the properties of ensemble-averaged zonal-mean zonal flows demonstrated in Takehiro *et al.* (2007). Fig.3 shows the ensemble average of the profiles of mean zonal flows over 50 members at the final point of numerical integration for each rotation rate. At $\Omega = 50$, the circumpolar easterly is located at the lower latitude and there is a circumpolar westerly flow near the pole. As the rotation rate is increased, the circumpolar easterly jet emerges with narrower and stronger features, and with its axis shifts poleward. Note that the banded structure in the low and mid-latitudes, which is observed in the individual distributions (Fig.2), is now invisible in the ensemble mean fields; it is smoothed out by the averaging process since their amplitude is weak and moreover the location and direction of mean zonal flow are different among the ensemble members. Only slight westerly flow biases can be observed in the low and mid-latitudes. Although the magnitude of the westerly bias decreases with increasing Ω , there does exist a westerly bias even for $\Omega = 10000$ to compensate the accumulation of the easterly angular momentum associated with the circumpolar jets.

[Figure 4 about here.]

The trend in change in the width and averaged velocity of the easterly circumpolar jet with increasing Ω is also shown in Fig.4. The strength of the jet is defined as the area mean easterly velocity over the circumpolar jet area, $\int_{\pi/2-\theta}^{\pi/2} |\bar{u}| \cos \varphi d\varphi / (1 - \cos \theta)$, where the jet is assumed to extend from the pole to the latitude $\pi/2 - \theta$ (θ is the colatitude, where the pole is indicated by $\theta = 0$, of the jet boundary). The equator-side boundary of the jet is defined as the latitude at which the cumulative integral of kinetic energy associated with the zonal mean component

$\int_{\pi/2-\theta}^{\pi/2} \frac{1}{2} \overline{u^2} \cos \varphi d\varphi$ changes its slope significantly. This definition of jet width is different from that of Takehiro *et al.* (2007) where the equator-side boundary is given as the latitude at which jet velocity is equal to the one-tenth of that at the jet's peak. The definition of Takehiro *et al.* (2007) tends to yield a smaller width.

[Figure 5 about here.]

[Figure 6 about here.]

Fig.5 and Fig.6 show the time development of zonally averaged wave quantities defined as linear Rossby waves for $\Omega = 400$ and $\Omega = 10000$, respectively. Note that these figures are equatorially symmetric because of the ensemble-mean process utilized, but we have kept both hemispheres to enable us to clearly recognize the contrast of behaviors between the polar caps and the other regions. The plotted quantities are wave activity (pseudo angular momentum associated with Rossby waves) $\overline{\zeta'^2} \cos \varphi / (2\hat{\beta})$, the latitudinal component of wave activity flux $-\overline{u'v'} \cos \varphi$, its divergence, and wave activity dissipation rate. Here $u = -\partial_\varphi \psi$ and $v = \partial_\lambda \psi / \cos \varphi$ are the longitudinal and latitudinal components of velocity, respectively, $\overline{\bullet}$ and $\bullet' = \bullet - \overline{\bullet}$ denote zonal mean and its deviation from the mean, respectively. $\hat{\beta} \equiv \partial_\varphi (2\Omega \sin \varphi + \bar{\zeta})$ is the latitudinal derivative of zonally averaged potential vorticity. Initially, as is apparent in Fig.5a, the distribution of wave activity is latitudinally uniform except for the polar regions where $\hat{\beta}$ is small. This is because the ensemble-mean amplitude of $\overline{\zeta'^2}$ is uniform over the sphere, and the behavior of $\hat{\beta}$ is roughly proportional to $2\Omega \cos \varphi$.

When $\Omega = 400$, the decrease in wave activity in the low and mid-latitudes is mostly caused by dissipation. Note that the tone interval of waveflux divergence shown in Fig.5b is 1/4 of that of wave activity dissipation shown in Fig.5d. The magnitude of wave activity which is latitudinally uniform in the low and mid-latitudes decreases also uniformly in the latitudinal direction and rapidly during the early stage of the integration up to around $t = 1$. The smooth distribution of decrease in magnitude the result of taking the the ensemble average; the distribution of each realization is significantly noisier. Even with the 50-ensemble average, wave activity convergence is still noisy as shown in Fig.5c.

An interesting feature of wave activity dissipation for $\Omega = 400$ is that it occurs not at the very beginning of the integration but reaches its maximum at around $t = 0.5$ (Fig.5d). That is the time when energy upcascade and enstrophy downcascade occur, and the banded structure of zonal flows begins to be established (not shown here). It seems that the development of the banded structure of zonal flows is caused locally by the Rhines effect on a local β -plane. The duration during which dissipation is active corresponds to the evolving period of the banded structure of zonal flows in the low and mid-latitudes. At around $t = 1$, the development of the banded structure of zonal flows in the low and mid-latitudes is almost completed (not shown here), and the most of the initial wave activity of these latitudes has ceased. The decrease in wave activity in the low and mid-latitudes in the next stage of integration is caused by the wave activity flux. The wave activity flux is poleward as indicated in Fig.5b. The development of poleward flux requires a bit of time from the initial state, It becomes evident at around $t = 1$, that is, after the end of the intense wave activity dissipation period described above, and lasts for

a fairly long time. Wave activity convergence occurs continuously at the high latitudes (Fig.5c).

The characteristic features of this poleward wave activity flux and its convergence can be recognized more clearly in the case of $\Omega = 10000$. With increasing Ω , the progress of the field development becomes faster. Now, for $\Omega = 10000$, The poleward flux becomes evident after around $t = 0.2$ (Fig.6b). The magnitude of flux continuously increases and reaches its maximum at around $t = 1$ at latitudes of around 75° . Then the maximum value decreases and the location of maximum moves toward lower latitudes. Fig.6a shows that accumulation of wave activity in the high latitudes occurs simultaneously with the establishment of the poleward wave activity flux. Wave activity increases around the latitudes where the flux converges (Fig.6c), but tends to decrease soon after. Correspondingly, wave activity dissipation is quite active in the polar regions (Fig.6d). This indicates that, as the Rossby waves reach those latitudes, they are quickly stirred and dissipated, and the easterly momentum associated with them is transformed into the mean zonal flow to enhance the easterly circumpolar jet there. As the easterly circumpolar jet grows, the latitude of the maximum convergence of wave activity flux shifts equatorward. This tendency indicates that the critical-level absorption of Rossby waves occurs in those latitudes.

It should be noted that, in Fig.6d for the case of $\Omega = 10000$, the wave activity dissipation at the early development stage in the low and mid-latitudes, which is prominent in Fig.5d for the case of $\Omega = 400$, is not evident. The decrease of wave activity in the low and mid-latitudes for $\Omega = 10000$ occurs mainly due to wave activity flux divergence. Dissipation is quite small in those latitudes compared to the magnitude of wave activity flux divergence. Note that the tone

intervals of wave activity flux divergence and wave activity dissipation in Fig.6 are the same. For $\Omega = 10000$, the initial energy spectral peak is not located at the wavenumber small enough for the field to be regarded as turbulent; this situation is similar to that of Yoden and Yamada (1993). The initial disturbances placed in the low and mid-latitudes propagate poleward as Rossby waves. Actually, the profile of zonal flows in the low and mid-latitudes shows little evolution from the initial profile for $\Omega = 10000$ (compare Fig.1c and Fig.2c).

The evolutionary features of wave activity, wave activity flux, its convergence, and dissipation in the polar caps after the initial rapid decrease of wave activity due to enstrophy cascade and dissipation do not depend qualitatively on the value of Ω . Because the disturbances produced by local energy upcascade or the disturbances placed initially are large enough, they can propagate poleward as Rossby waves from the low and mid-latitudes toward the polar caps, where they are absorbed to produce the circumpolar easterly jets. The quantitative difference is that, as the Ω decreases, the evolution of wave activity flux progresses more slowly, accumulation of easterly momentum toward the polar regions lasts longer, and its maximum appears at the lower latitude.

5. Theoretical model of kinetic energy accumulation

One of the important aspects found by Takehiro *et al.* (2007) is that the total kinetic energy of the system is asymptotically concentrated into the easterly circumpolar jets as Ω increases. For all cases of Ω , total kinetic energy, which is defined as the integral of kinetic energy over the

whole sphere, $E_{total} \equiv \int dS |\nabla \psi|^2 / 2$, decreases only 10 percent during the integration period. The eddy component of total kinetic energy, $E_{eddy} \equiv \int dS |\nabla \psi'|^2 / 2$, is dominant in the initial stage, but is gradually converted into the zonal mean component, $E_{zonal} \equiv \int dS |\nabla \bar{\psi}|^2 / 2$. This tendency is consistent with the absorption of Rossby waves into the mean zonal flows inferred by the analysis of wave activity. At the final state, when the time variation of each component becomes small and kinetic energy conversion process is nearly completed, the ratio of the zonal mean component to the eddy component increases as the rotation rate is increased. Especially, when $\Omega \geq 1000$, nearly all of the kinetic energy is concentrated in the zonal mean component as seen clearly in Fig.7. Since the amplitude of the zonal flow in the low and mid-latitudes is small for $\Omega \geq 1000$, the zonal mean component of kinetic energy is attributed to the circumpolar jets.

[Figure 7 about here.]

These tendency of kinetic energy may be interpreted as follows: Among the initial vortices distributed over the whole sphere, vortices in the polar region interact to each other without influence of the β effect and there is no reason for kinetic energy there to be biased to the zonal component. As a result, they continue to contribute to the disturbance component of kinetic energy. In contrast, the β effect dominates the vortices in the low and mid-latitudes, which therefore behave as Rossby waves. These Rossby waves propagate poleward and are absorbed into the circumpolar easterly jets. Most of the energy existing in the low and mid-latitudes is also carried out associated with these Rossby waves from these latitudes to the polar caps. As Rossby waves are absorbed into the circum polar jets in the polar regions, the associated energy from the low and mid-latitudes is also converted into the mean zonal component of

kinetic energy. Thus, kinetic energy of the initial vortices existing in the latitudes lower than the latitudes of the circumpolar jets accumulates into the zonal mean component in the final state.

The important simplification assumed here is that the initial disturbances placed inside of the final circum polar easterly jet area do not contribute to its angular momentum accumulation, while all of the energy in the low and mid-latitudes outside of the polar caps is converted into the circumpolar jets. The assumption is that circumpolar jets are intensified only through the propagation and absorption of Rossby waves from the low and mid-latitudes. Disturbances in the polar caps may contribute to determining the detailed profile of the polar jets, but they are assumed to remain in existence and to not be absorbed into the zonal mean flows. On the other hand, the energy remaining as the banded structure of zonal flows in the low and mid-latitudes is assumed to be negligible compared to the energy carried out by Rossby waves.

Following this hypothesis, let us construct a theoretical model for finding the accumulation of the zonal mean component of kinetic energy and the averaged velocity and width of the circumpolar jet as functions of the rotation rate. Let us suppose that the easterly circumpolar jet extends from the pole to the colatitude θ , where θ is the latitudinal width of the jet. Firstly, we assume that In the polar region, where non-linear interaction dominates, the jet spreads around the pole by the local Rhines length scale to the south. Using the local Rhines wavenumber, this can be expressed as

$$k_{Rhines} = \frac{2\pi}{a\theta/2} = \sqrt{\frac{\beta(\theta/2)}{U_p}} = \sqrt{\frac{2\Omega \sin(\theta/2)}{U_p a}},$$

which gives

$$\frac{U_p}{2\Omega a} = \frac{1}{4\pi^2} \left(\frac{\theta}{2}\right)^2 \sin\left(\frac{\theta}{2}\right). \quad (4)$$

The local Rhines scale is evaluated around the center of the circumpolar jet. U_p is the mean magnitude of the circumpolar jet velocity averaged over the jet extent, $\beta(\theta/2)$ is the β parameter at the colatitude $\theta/2$, and a is the radius of the sphere, which is equal to unity in our experiments.

The second assumption is that the initial vortices existing outside of the circumpolar jet region contribute to the kinetic energy of the circumpolar jet, and this is almost equal to the zonal mean component of kinetic energy in the final state \hat{E}_{zonal} .

$$\hat{E}_{zonal} = 4\pi \int_{\pi/2-\theta}^{\pi/2} \frac{1}{2} U_p^2 \cos \varphi d\varphi = 4\pi \int_0^{\pi/2-\theta} \frac{1}{2} U_0^2 \cos \varphi d\varphi, \quad (5)$$

where U_0 is a typical velocity scale of the initial vortices, which is equal to $\sqrt{2}$ in our experiments because the initial state is given so that the averaged kinetic energy becomes unity. From Eq.5, we obtain

$$\hat{E}_{zonal} = 2\pi U_0^2 \cos \theta, \quad U_p^2 = U_0^2 \frac{\cos \theta}{1 - \cos \theta}. \quad (6)$$

Eqs.4 and 6 yield the dependences of \hat{E}_{zonal} , U_p and θ on the rotation rate Ω .

The dotted line in Fig.7 shows the estimated mean zonal component of kinetic energy \hat{E}_{zonal} , which agrees fairly well with the results of numerical experiments. Note that since the total kinetic energy decreases by about 10% at the final stage, the estimate becomes larger than the calculated total kinetic energy when Ω is large. The broken and dotted lines in Fig.4 are

the estimated averaged velocity and width of circumpolar jets, respectively. Both of the lines explain well the dependences on the rotation rates.

Particularly, when the rotation rate is large, θ becomes small. Under the approximation of small θ , we obtain

$$\frac{U_p}{2\Omega a} \sim \frac{1}{4\pi^2} \left(\frac{\theta}{2}\right)^3. \quad (7)$$

From Eq.6, we can approximate $U_p^2 \sim 2U_0^2/\theta^2$, and then we have,

$$U_p \sim \frac{(\sqrt{2}U_0)^{3/4}}{\sqrt{2\pi}} (2\Omega a)^{1/4}, \quad (8)$$

which shows that the strength of the jets is proportional to the one-fourth power of the rotation rate. On the other hand, the width of the jet is calculated as,

$$\theta \sim 2\sqrt{2\pi}(\sqrt{2}U_0)^{1/4}(2\Omega a)^{-1/4}. \quad (9)$$

The jet width is proportional to the minus one-fourth power of the rotation rate. We can also reproduce the asymptotic feature of circumpolar jets at the large rotation rate, which was previously obtained in Takehiro *et al.* (2007).

It may be worth mentioning here the roughness of the above argument. It may be argued that the dynamic transition from wavy to turbulence should occur at the equator-side boundary of the jet, and hence, the evaluation should be made at θ rather than $\theta/2$. It may also be argued that the velocity scale in estimating the Rhines wavenumber should be random velocity

rather than the mean jet velocity. We are omitting these levels of differences. According to our calculation results, the velocity scale seems to be smaller than the mean jet velocity, but to be larger than the initially given random velocity. We have adopted U_p simply because we have no other simple measure. Moreover, a similar θ -dependence for the leading order of U_p as seen in Eq. 4 can also be obtained from several different assumptions. For instance, based on considerations of the critical latitude absorption of Rossby waves, U_p may be assumed to be equal to the phase velocity of Rossby waves whose wavenumber is on the order of the jet width (a quantitative argument is given in Hayashi *et al.* 2000). However, the issue here is whether the present choice of wavenumber may be justified. Based on considerations of the homogenization of potential vorticity in the polar jet, the latitudinal profile of zonal-mean zonal wind \bar{u} may be directly obtained. More simply, in order to compensate the variation of planetary vorticity by the relative vorticity associated with the established circumpolar jet, we have $U_p(2\pi/\theta/2)^2 \sim 2\Omega \sin(\theta/2)$ (note again that factors are rather arbitrary). However, now the problem is that, according to our numerical results, potential vorticity in the polar jet region is not so homogeneous, especially when Ω is large. As is indicated in Fig. 8, potential vorticity is extensively mixed over the circumpolar jet region for $\Omega = 400$, while it is not as extensive for $\Omega = 10000$. Turbulent mixing in the polar caps is weak for large Ω cases. We suspect that the accumulation of momentum into the polar caps has, to a certain extent, the nature of critical latitude absorption, rather than the fully nonlinear Rhines effect. In order to develop a more sophisticated argument, it seems that we will need to reconstruct and refine the argument thoroughly from the beginning.

[Figure 8 about here.]

6. Summary

As an extension of the study of Takehiro *et al.* (2007), we have performed numerical experiments of two-dimensional freely decaying barotropic turbulence on a rotating sphere for cases of larger rotation rates than those employed previously. Numerical time integrations were carried out for sufficiently long periods until the mean zonal component of kinetic energy is fully developed. The results have confirmed the emergence of easterly circumpolar jets and the banded structure of zonal flow in the low and mid-latitudes. The intensity of the established zonal flows is extreme inhomogeneous with respect to the latitude: Easterly circumpolar jets are quite strong, whereas zonal flows in the low and mid-latitudes are relatively weak and unanimously westerly biased to compensate the easterly angular momentum accumulation in the polar caps. As the rotation rate is increased, this inhomogeneity is intensified: Easterly circumpolar jets are concentrated in the polar region and their velocity profile is sharpened and strengthened, while the amplitude of the zonal banded structure in the low and mid-latitudes decreases in association with their narrowing.

The wave activity analysis clarified the evolution of zonal mean flows and the formation of circumpolar jets from the perspective of Rossby waves. The development of the banded structure of zonal flows in the low and mid-latitudes are associated with the large dissipation of wave activity, and hence can be regarded as caused by the local upcascade of energy and

the Rhines effect of the local β plane. Then, the disturbances in the low and mid-latitudinal region continuously propagate poleward as Rossby waves, and they are absorbed at the polar regions resulting in the enhancement of the easterly circumpolar jets there. Simultaneously, vortex motions and banded zonal flow formation in the low and mid-latitudes become inactive. As a result, total kinetic energy tends to be accumulated into the easterly circumpolar jets. In particular, nearly all of the kinetic energy is concentrated in the circumpolar jets when the rotation rate is large.

By applying the assumptions that the location of the circumpolar jets is determined by the latitude where the non-linear term and the β term of the vorticity equation balances and that the kinetic energy of the initial vortices existing in the latitudinal region lower than the latitudes of the circumpolar jets contribute to that of the jets, we have succeeded in theoretically finding the dependence of the mean zonal component of kinetic energy and the averaged velocity and width of the jets on the rotation rate. These theoretical estimates agree fairly well with the numerical results. In particular, the asymptotic limit of large rotation rates for this theory shows that the strength and width of the jets are in proportion to one-fourth and minus one-fourth powers of the rotation rate, respectively. This asymptotic feature is consistent with the results by Takehiro *et al.* (2007).

Note that the inhomogeneity of banded structure of zonal flows inherent in the two-dimensional barotropic decaying turbulence on a rotating sphere, which is clearly shown in this study, does not appear in the framework of two-dimensional β -plane whose governing vorticity equation is latitudinally homogeneous. Caution should be exercised when applying conclusions regarding

banded structures of zonal flows obtained in β -plane cases to rotating sphere cases, or when applying them to the actual planetary atmospheres. This may lower the significance of the studies performed so far about the origin and maintenance of the zonal banded structure of the atmospheres of Jovian planets discussed within the framework of two-dimensional flows on a β plane. Latitudinal inhomogeneity of the β effect may be indispensable. On the other hand, we should also bear in mind the possibility that some other effects are involved in the inhibiting the dominance of inhomogeneous banded structure. If the amplitude of zonal banded flows in the low and mid-latitudes is sufficiently large from the beginning, or is maintained by small scale forcing, the zonal flows may prevent the propagation of the Rossby waves to higher latitudes and the subsequent accumulation of kinetic energy into the circumpolar jets. The forced turbulence cases on a rotating sphere exemplified by Nozawa and Yoden (1997a,b) and Huang and Robison (1998) might be such cases. Continuously excited vortices might enhance in-situ jets and cause homogeneous global banded structures.

Acknowledgments

All comments by the reviewers would be greatly appreciated by the authors. This work was supported by Grants-in-Aid for Scientific Research of the Japan Society for the Promotion of Science. Numerical computations were carried out on VPP5000 at the Astronomical Data Analysis Center of the National Astronomical Observatory, Japan, and on HPC2500 at the Academic Center for Computing and Media Studies of Kyoto University, Japan. The main part of

the numerical model used in this study was constructed with a spectral transformation library “ISPACK” (<http://www.gfd-dennou.org/library/ispack/>) and a Fortran90 wrapper library “SP-MODEL” (<http://www.gfd-dennou.org/library/spmodel/>). “gt4f90io” (<http://www.gfd-dennou.org/library/gtool4/>) and “NetCDF” (<http://www.unidata.ucar.edu/packages/netcdf/>) libraries were used for data IO routine of the model. Data analysis and visualization were done using the software products of the GFD Dennou Ruby project (<http://ruby.gfd-dennou.org/>).

References

- F. H. Busse, , 1983: Convection-driven zonal flows in the major planets. *PAGEOPH*, **121**, 375–390.
- Cho, J. Y-K. and L. M. Polvani, 1996: The emergence of jets and vortices in freely evolving, shallow-water turbulence on a sphere. *Phys. Fluids*, **8**, 1531–1552.
- Hayashi, Y.-Y., Ishioka, K., Yamada M., and S. Yoden, 2000: Emergence of circumpolar vortex in 2-D turbulence on a rotating sphere. *IUTAM Symposium on Developments in Geophysical Turbulence (Proceedings of the IUTAM Symposium held at the National Center for Atmospheric Research, Boulder, CO, 16-19 June 1998)* (Fluid Mechanics and Its Applications Vol.58), Kerr R. M. and Y. Kimura Ed., Kluwer Academic Publishers, 179–192.
- Hayashi, Y.-Y., Nishizawa, S., Takehiro, S., Yamada M., Ishioka, K., and S. Yoden, 20007: Rossby waves and jets in a two-dimensional decaying turbulence on a rotating sphere. *J. Atmos. Sci.*, (submitted).
- Heimpel, M., Aurnou, J., and J. Wicht, 2005: Simulation of equatorial and high-latitude jets on Jupiter in a deep convection model. *Nature*, **438**, 193–196.
- Huang, H.-P. and Robinson, W. A., 1998. Two-dimensional turbulence and persistent zonal jets in a global barotropic model. *J. Atmos. Sci.*, **55**, 611–632.
- Ishioka K., Yamada M., Hayashi Y.-Y. and S. Yoden 1999: Pattern Formation from

- Two-dimensional Decaying Turbulence on a Rotating Sphere, *Nagare Multimedia* 99, <http://www.nagare.or.jp/mm/99/ishioka/>.
- Ishioka, K., Yamada, M., Hayashi, Y.-Y., S. Yoden, 2000: Technical approach for the design of a high-resolution spectral model on a sphere: application to decaying turbulence. *Nonlinear Processes in Geophysics*, **7**, 105–110.
- Li, S. and D. Montgomery, 1996: Decaying two-dimensional turbulence with rigid walls. *Physics Letters A*, **218**, 281–291.
- Li, S. and Montgomery, D. 1997: Two-Dimensional Turbulence with Rigid Circular Walls, *Theoret. Comput. Fluid Dynamics* **9**, 167–181.
- Nozawa, T. and S. Yoden, 1997a: Formation of zonal band structure in forced two-dimensional turbulence on a rotating sphere. *Phys. Fluids*, **9**, 2081–2093.
- Nozawa, T. and S. Yoden, 1997b: Spectral anisotropy in forced two-dimensional turbulence on a rotating sphere. *Phys. Fluids*, **9**, 3834–3842.
- P. B. Rhines, 1975: Waves and turbulence on a beta-plane. *J. Fluid Mech.*, **69**, 417–443.
- Takehiro, S., Odaka, M., Ishioka, K., Ishiwatari, M., Hayashi, Y.-Y. and SPMODEL Development Group, 2006: SPMODEL: A series of hierarchical spectral models for geophysical fluid dynamics. *Nagare Multimedia* 2006, <http://www.nagare.or.jp/mm/2006/spmodel/>.
- Takehiro, S., Yamada, M., and Y.-Y. Hayashi, 2007: Circumpolar jets emerging in two-

dimensional non-divergent decaying turbulence on a rapidly rotating sphere. *Fluid Dyn. Res.* (to appear).

Taniguchi, Y., Yamada, M. and K. Ishioka, 2002: Flow pattern formation in a two-dimensional flow on the rotating hemisphere bounded by the meridional line. *Proceedings of the 51st Japan National Congress for Theoretical and Applied Mechanics*, K. Uetani, Ed., **51**, 217–223.

G. P. Williams, 1978: Planetary circulations: 1. Barotropic representation of Jovian and terrestrial turbulence, *J. Atmos. Sci.*, **35**, 1399–1426.

Yoden, S. and M. Yamada, 1993: A numerical experiment on two-dimensional decaying turbulence on a rotating sphere. *J. Atmos. Sci.*, **50**, 631–643.

Yoden, S., Ishioka, K., Hayashi, Y.-Y., and M. Yamada, 1999: A further experiment on two-dimensional decaying turbulence on a rotating sphere. *Il Nuovo Cimento*, **22 C**, 803–812.

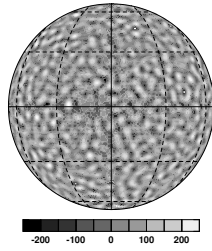
Yoden, S., Ishioka, K., Yamada, M., and Y.-Y. Hayashi, 2002: Pattern formation in two-dimensional turbulence on a rotating sphere. *Statistical Theories and Computational Approaches to Turbulence*, Kaneda Y. and T. Gotoh, Ed., Springer-Verlag, Tokyo, 317–326.

List of Figures

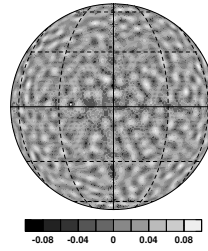
1	An example of the initial states.	30
2	Examples of the fields for various values of Ω using Fig.1 as the initial state. Left panels show relative vorticity at the final states. Orthographic projection from the equator is used. Right panels are the profiles of relative angular momentum. Solid and broken lines represent the profiles in the final states and at $t = 5$, respectively.	31
3	Zonal mean flow profiles obtained from the average of 50 ensemble members (reproduction of Takehiro <i>et al.</i> , 2007). (a) Solid, long-dashed, short-dashed, and dash-dotted lines denote the cases of $\Omega = 0, 50, 100, 200$, respectively. (b) Solid, long-dashed, short-dashed, and dash-dotted lines denote the cases of $\Omega = 400, 1000, 4000, 10000$, respectively.	32
4	Dependence of width (asterisk) and strength (circle) of the ensemble averaged circumpolar easterly jet on rotation rate Ω . Dotted and broken lines are the width and strength estimated by the theoretical model described in Sec.5, respectively.	33
5	Time development of zonal mean wave quantities averaged over 50 ensemble members from $t = 0$ to 10 for $\Omega = 400$. (a) latitudinal component of wave activity flux, (b) wave activity, (c) wave activity flux divergence, and (d) wave activity dissipation. Note that the tone interval for (d) is 4 times that of (c).	34

6	Same as Fig.5but for $\Omega = 10000$. Note that the tone interval for (a) is 1/25 of that in Fig.5, and the tone interval for (d) is now the same as that of (c).	35
7	Dependence of total (circle) and zonal mean part (asterisk) of kinetic energy in the final state for the rotation rate Ω . Dotted line shows the estimate of zonal mean part of kinetic energy described in Sec.5.	36
8	Zonal mean potential vorticity gradient profile obtained from the average of 50-ensemble members. (a) $\Omega = 400$, (b) $\Omega = 10000$	37

(a) Vorticity.



(b) Stream function.



(c) Relative angular momentum. (d) Kinetic Energy spectrum.

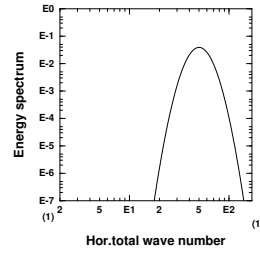
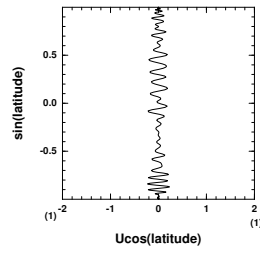


Figure 1: An example of the initial states.

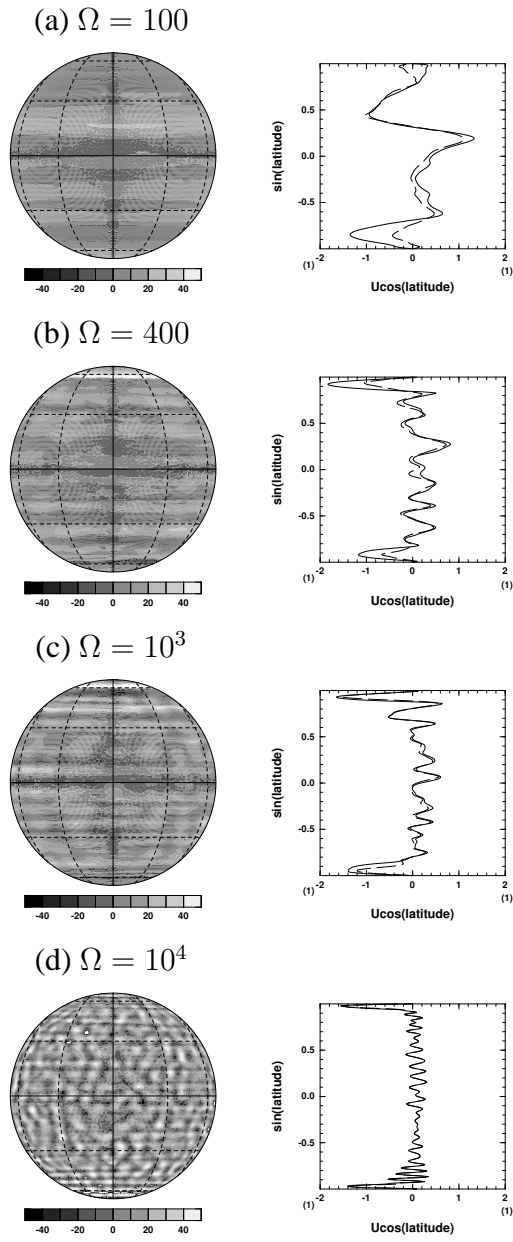


Figure 2: Examples of the fields for various values of Ω using Fig.1 as the initial state. Left panels show relative vorticity at the final states. Orthographic projection from the equator is used. Right panels are the profiles of relative angular momentum. Solid and broken lines represent the profiles in the final states and at $t = 5$, respectively.

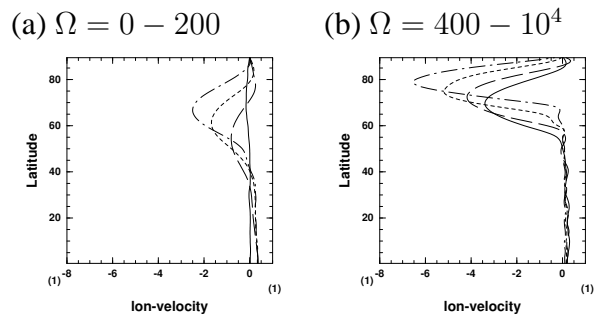


Figure 3: Zonal mean flow profiles obtained from the average of 50 ensemble members (reproduction of Takehiro *et al.*, 2007). (a) Solid, long-dashed, short-dashed, and dash-dotted lines denote the cases of $\Omega = 0, 50, 100, 200$, respectively. (b) Solid, long-dashed, short-dashed, and dash-dotted lines denote the cases of $\Omega = 400, 1000, 4000, 10000$, respectively.

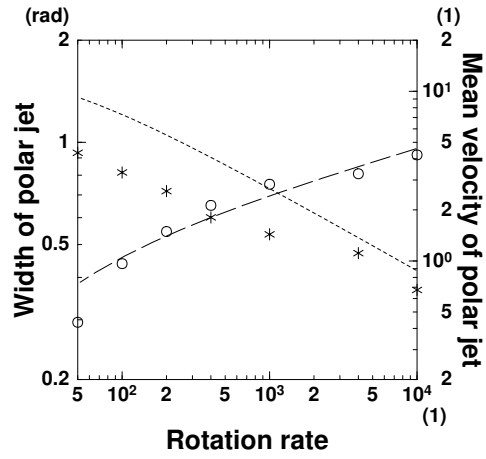
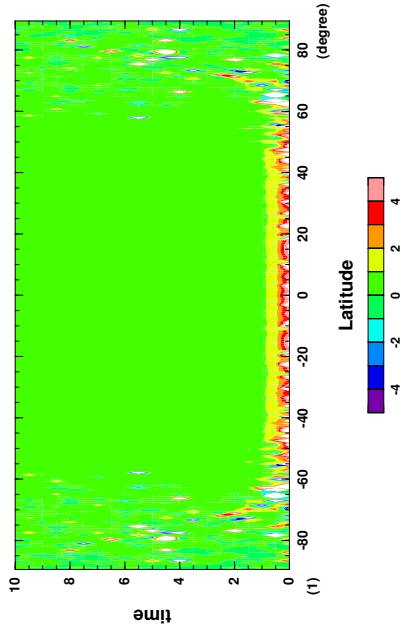
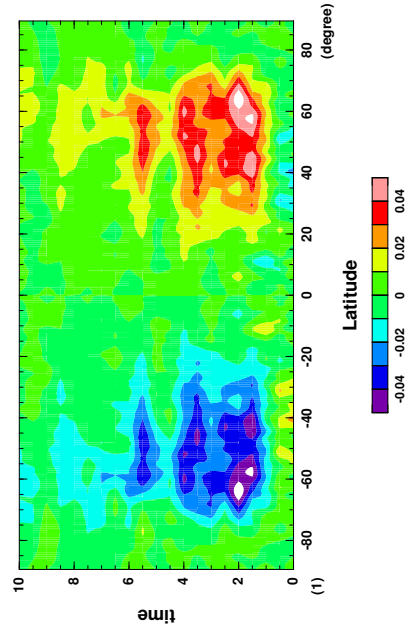


Figure 4: Dependence of width (asterisk) and strength (circle) of the ensemble averaged circumpolar easterly jet on rotation rate Ω . Dotted and broken lines are the width and strength estimated by the theoretical model described in Sec.5, respectively.

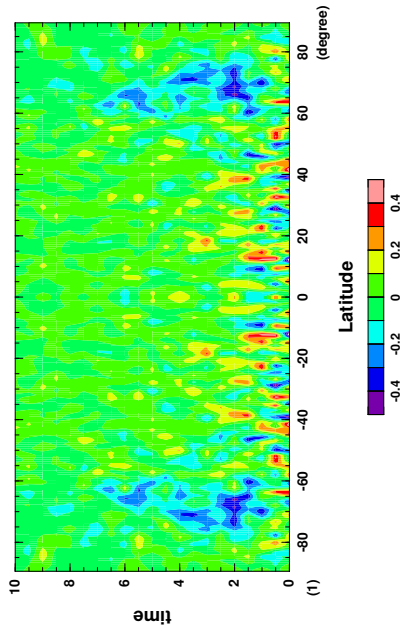
(a) Wave activity



(b) Wave activity flux



(c) Wave activity flux divergence



(d) Wave activity dissipation

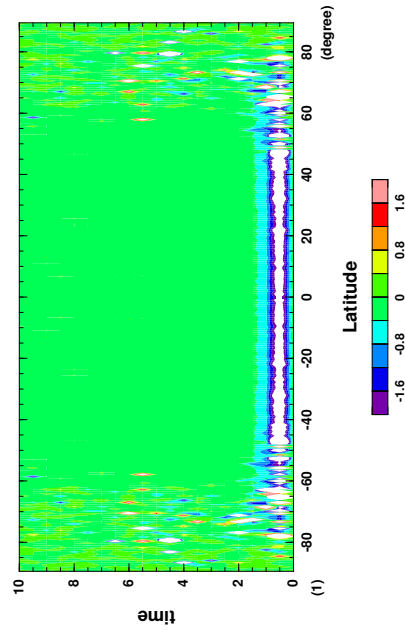
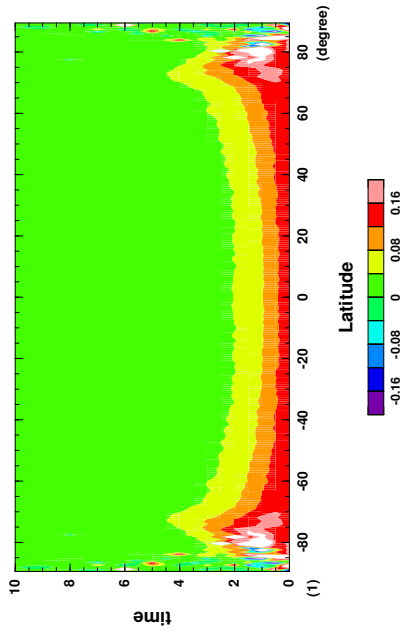
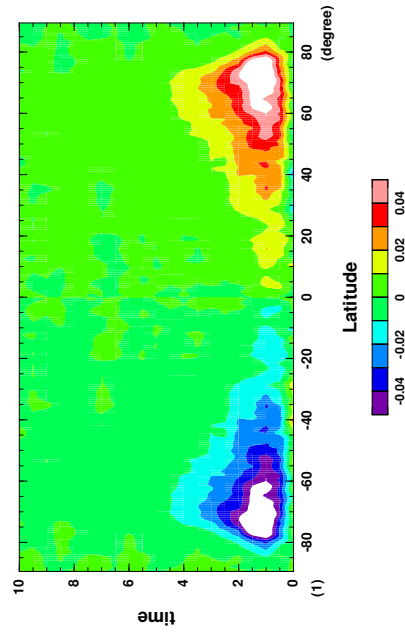


Figure 5: Time development of zonal mean wave quantities averaged over 50 ensemble members from $t = 0$ to 10 for $\Omega = 400$. (a) latitudinal component of wave activity flux, (b) wave activity, (c) wave activity flux divergence, and (d) wave activity dissipation. Note that the tone interval for (d) is 4 times that of (c).

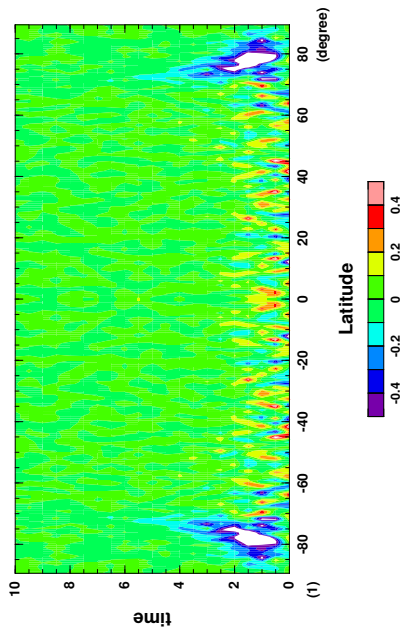
(a) Wave activity



(b) Wave activity flux



(c) Wave activity flux divergence



(d) Wave activity dissipation

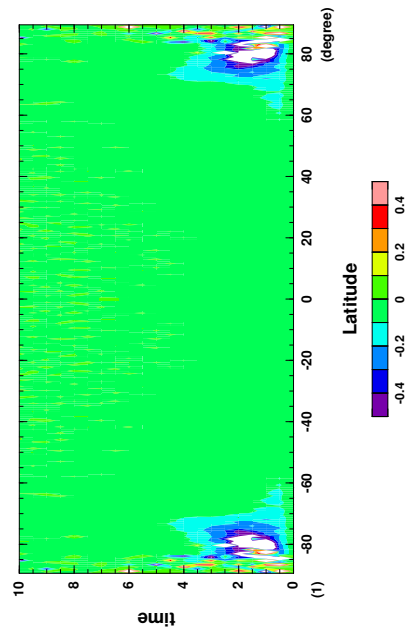


Figure 6: Same as Fig.5 but for $\Omega = 10000$. Note that the tone interval for (a) is $1/25$ of that in Fig.5, and the tone interval for (d) is now the same as that of (c).

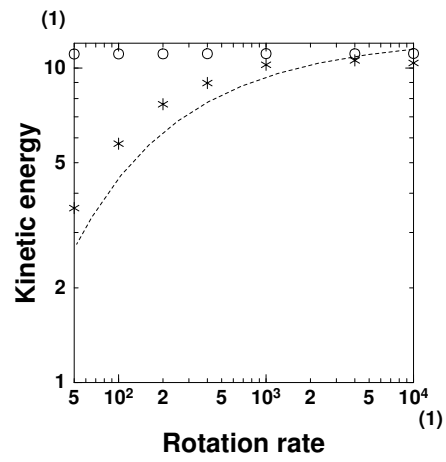
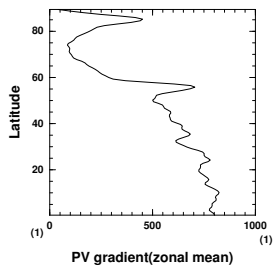


Figure 7: Dependence of total (circle) and zonal mean part (asterisk) of kinetic energy in the final state for the rotation rate Ω . Dotted line shows the estimate of zonal mean part of kinetic energy described in Sec.5.

(a) $\Omega = 400$



(b) $\Omega = 10^4$

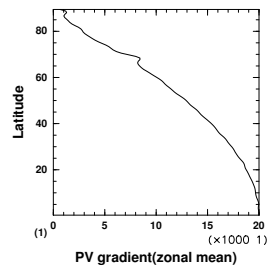


Figure 8: Zonal mean potential vorticity gradient profile obtained from the average of 50-ensemble members. (a) $\Omega = 400$, (b) $\Omega = 10000$.

List of Tables

- 1 Values of time increment Δt , length of time integration t_{final} , and characteristic wavenumber $n_\beta = \sqrt{\pi\Omega/\sqrt{2\mathcal{E}}}$ for each value of the rotation rate Ω 39

Table 1: Values of time increment Δt , length of time integration t_{final} , and characteristic wavenumber $n_\beta = \sqrt{\pi\Omega/\sqrt{2\mathcal{E}}}$ for each value of the rotation rate Ω .

Ω	Δt	t_{final}	n_β
0	1×10^{-3}	5	0
50	1×10^{-3}	80	5.27
100	1×10^{-3}	80	7.45
200	1×10^{-3}	40	10.5
400	1×10^{-3}	20	14.9
10^3	4×10^{-4}	20	23.6
4×10^3	1×10^{-4}	20	47.1
10^4	4×10^{-5}	10	74.5